Acta Geotechnica (2006) 1:43–57
DOI 10.1007/s11440-006-0005-9

RESEARCH PAPER

Adaptive finite element analysis of cone penetration in clay

J. Walker · H. S. Yu

Received: 13 October 2005 / Accepted: 22 December 2005 / Published online: 21 April 2006

Abstract This paper presents a numerical technique for the analysis of the cone penetration test by means of the commercial finite element code ABAQUS. The von Mises yield criterion with its associated flow rule is assumed to model the plastic behaviour of elastoplastic undrained clays. An explicit finite element scheme is used to efficiently perform a large number of loading increments and to simplify the treatment of contact. An Arbitrary Langrangian–Eulerian (ALE) scheme is adopted to preserve the quality of mesh throughout the numerical simulation. A volumetric weighting algorithm adjusts the relative positions of nodes after each loading increment. This prevents mesh over distortion and allows the simulation to run continuously. The variation of the cone resistance is examined in relation to various parameters such as the in situ stress state, shaft and cone face roughness, and the material strength when steady state conditions have been reached. The trends of these variations are highlighted and compared with those found by other researchers. This technique can be extended to analyse the plastic behaviour of elastoplastic sands often modelled using either the Drucker–Prager yield criterion or a critical state model.

Keywords Cone penetration · Finite element analysis · ABAQUS · Arbitrary Langrangian–Eulerian (ALE) scheme

J. Walker · H. S. Yu (✉)
Nottingham Centre for Geomechanics, School of Civil Engineering, The University of Nottingham, University Park, NG7 2RD Nottingham, UK
E-mail: hai-sui.yu@nottingham.ac.uk

1. Introduction

Over the last few decades, cone penetration testing (with or without pore pressure measurement, i.e. CPTU or CPT, respectively) has been established as the most widely used in situ testing device for obtaining soil profiles. The popularity of this in situ testing device has resulted in a great demand for the effective assessment of correlations between measured cone quantities and engineering properties of soils. Recent reviews presented by Yu and Mitchell [30] and Lunne et al. [19] suggest that despite much research, rigorous solutions to the deep penetration problem in soils are still unavailable. Due to the importance of deep penetration in foundation engineering and the increasing reliance on in situ tests for soil profiling in offshore engineering, the effective analysis of deep cone or pile penetration in soils still represents a significant challenge to the geotechnical community.

It has long been realised that the interpretation of in situ tests is beset with difficulties especially if the results are needed to assess the stress-strain and strength characteristics of soils [27, 29]. These difficulties arise because of the complicated soil deformation resulting from the punching of the penetrometer. Many in situ tests, including the CPT/CPTU represent complex boundary value problems rendering their theoretical interpretation difficult. Given that the interpretation of an in situ test requires the analysis of a corresponding boundary value problem, some simplifying assumptions have to be made. Hence, most existing cone resistance correlations have been obtained by using one (or more) of the following approaches: Bearing Capacity Theory, Cavity Expansion Theory, Steady-State Deformation Theory, Incremental Finite Element Analysis or Calibration Chamber Testing.

The finite element (FE) method has played an important role in the analyses of geotechnical problems since its first application to geotechnical engineering in the analysis of embankments. The finite difference and the finite element methods can provide a full numerical analysis where all the numerical requirements including realistic constitutive models and boundary conditions are satisfied, albeit in a numerically approximate manner. However, the application of a full finite element analysis is not always straightforward and at present, the simulation of large deformations still remains a challenging issue. In geotechnical engineering, there are two FE approaches dealing with problems of large deformation, namely Lagrangian and Eulerian formulations. Both of these methods are based on the fundamental theories of continuum mechanics and try to take into account the effects of displacement, strain, material rotation and the consequent changes in loading condition. Either formulation is theoretically capable of including the various effects of large strain deformation into its governing equations. However, practically this is difficult to achieve and therefore, no general and rigorous formulation is currently available.

A large strain formulation is essential because, as pointed out by Houlsby et al. [12], conventional small strain finite element analysis (e.g. [8]) is unable to generate the necessary stress field around the cone and thus fails to achieve an appropriate cone resistance. A review by Yu and Mitchell [30] suggested that many previous large strain, incremental finite-element analyses have treated the CPT as a collapse load problem (see [5] for clays and [7] for sand). In these analyses, zero thickness elements were used to model the frictional interface between the cone and the soil allowing the interface roughness to be varied. Van den Berg [24] noted that when using these models, it was necessary to decide the new location of boundary nodes after each loading step and when the roughness of the penetrometer is modelled, this procedure becomes very complicated and the robustness of the whole numerical procedure is not clear.

Sheng et al. [21] presented a finite element analysis of the cone penetration test in a cohesive soil. Contact elements capable of large scale sliding along the penetrometer surface were used to model the whole penetration process from the ground surface to a prescribed depth. The emphasis of their study was on pore pressure development around the cone at different penetration speeds.

An alternative approach to a large deformation analysis is an Eulerian scheme where the element mesh is fixed and the material flows through the elements [24]. However, this approach has some mathematical difficulties in the calculation of material time derivatives.

To avoid frequent remeshing in a large strain finite element calculation, Van den Berg [24] used an Arbitrary Lagrangian–Eulerian (ALE) formulation to uncouple nodal displacements and velocities from material displacements and velocities. The uncoupling of material and nodal displacements requires the advection of field variables between the old mesh and the new mesh. One of the first advection methods able to do this was presented by Huetink [14, 15]. The basic idea was to introduce additional continuous stress and strain fields by interpolating nodal stresses and strains. The advective terms were then calculated as the product of the gradients of these additional field variables and the displacement increments. However, it was found that this first order advection scheme diminished the strain gradients and this implied that the advective increment disappeared. To overcome this problem, so-called ‘local’ or ‘global’ smoothing procedures described by Huetink [15] were introduced. Unfortunately, the use of these simple smoothing procedures did not always give stable and accurate solutions.

Hu and Randolph (1998a) presented a technique referred to as the RITSS (Remeshing and InTerpolation with Small Strain) model. In this approach, a series of small strain analysis increments were followed by the complete remeshing and interpolation of field quantities (stress and material properties) between the old mesh and the new mesh. Hu and Randolph (1998a, b) discussed five approaches for the advection of the field variables and concluded that the (Modified) Unique Element Method was most suitable. This has allowed a full, large strain analysis of the cone penetration test in a simple elastic, perfectly plastic Tresca material to be simulated and it has been successfully performed by Lu [18].

This paper presents the full finite element analysis of the deep penetration of a cone penetrometer into homogenous, undrained clay. The undrained clay is modelled using perfect plasticity, the von Mises failure criterion and an associated flow rule. An ALE analysis is used and the field variables are transferred between meshes using a second order advection technique [25]. The advection of momentum is carried out using the Half Shift Index method [4]. This advection method is monotonic and consistent.

The presented investigation examines what effects the rigidity index of the material, the cone and shaft roughness, and the in situ stress state have on the resistance to penetration. The results are compared with those from other researchers. Preliminary tests have shown that the proposed technique can be extended to model frictional-dilatant materials using the Drucker–Prager failure criterion.

2. FE analysis for continuous penetration

2.1. Introduction

This section explains the procedures used to simulate the penetration of a cone penetrometer from the soil surface to any depth. This is achieved using both the explicit dynamics procedure and the adaptive meshing tool in the commercial finite element software ABAQUS.

The explicit dynamics procedure performs a large number of small time increments efficiently and uses a central difference time integration rule. The procedure requires no iterations, no tangent stiffness matrix and a solution to a set of simultaneous equations is not required. Each increment is relatively inexpensive because lumped element mass matrices are used. However, the resulting formulation is only conditionally stable and the increment size is dictated by the stability limit.

The explicit procedure is ideally suited to analysing high speed dynamic events but many of the advantages of the explicit procedure also apply to the analysis of slower (quasi-static) processes. This is particularly true in cases where contact dominates a solution and local instabilities may form as a result.

2.2. Treatment of contact

This section will describe how this simulation establishes contact and calculates the resulting deformation in the model.

In ABAQUS, the contact algorithm is based on the concept of a master surface and a slave surface. The master surface pushes into the slave surface and contact forces are generated to prevent nodes penetrating into the master surface. Contact is established with contact pairs which use a kinematic contact algorithm that enforces contact constraints and conserves momentum.

At the start of each increment, the kinematic state of a model is advanced into a predicted configuration without considering the contact conditions. The slave nodes that penetrate the master surface are then determined and the depth of each node's penetration, the mass associated with it and the time increment are used to calculate the force necessary to resist the penetration. If this force had been applied during the increment it would have caused the slave node to exactly contact the surface.

The resisting force at each slave node is defined using a hard contact condition (as opposed to a penalty contact condition). This is a common contact condition where no pressure is transmitted between the surfaces when the nodes are not in contact. When the surfaces are in contact, any contact pressure can be transmitted between them. The surfaces separate when the contact pressure reduces to zero.

Movement between surfaces in contact is modelled by a finite sliding algorithm that allows for any arbitrary motion of the surfaces. In this study, both smooth and rough conditions are adopted at the contact interface. In smooth cases, a completely frictionless condition exists at the contact interface. The rough condition is modelled with a 'sticky' condition existing at the contact interface until a limiting shear stress is reached and under this condition, the soil is allowed to slide freely along the interface. The 'sticky' condition is reapplied if the shear stress at the contact interface falls below the preset limit value.

A contact search algorithm is used to detect contact. The algorithm uses both a global search and a local search procedure to provide a balance between accuracy and computational speed. A global search is used at the beginning of each step and a hierarchical global/local search algorithm is used throughout the step.

A global search determines the nearest master surface facet for each slave node in a contact pair. A bucket sorting algorithm is used to minimise the computational expense of these searches. An example is shown in Figure 1.

The global search computes the distance from node 50 to all the master surface facets in the same bucket as node 50. It determines the facet on the master surface that is closest to node 50, this is the facet of element 10. Node 100 is the node on this facet that is closest to node 50 and it is designated as the tracked master surface node. This search is conducted for each slave node by comparing each node against all of the facets on the master surface that are in the same bucket. Despite the bucket-sorting algorithm, global searches are computationally expensive.

A local search is used to track the motion of surfaces during the analysis. If Fig. 1 is advanced by one increment, then a given slave node (node 50 in this case) searches only the facets that are attached to the tracked master surface node (i.e. facets 9 and 10). Of these, the facet which is closest to the slave node is determined. The node on this facet which is closest to the slave node is considered the new tracked master surface node (node 101 in this case, see Fig. 2). If the master surface node has changed another iteration of the search is performed. This procedure can be understood more clearly using Fig. 2.

Let us suppose that the translation of the slave surface shown in Figure 2 occurs over one increment. The first iteration of the local search finds that of the facets attached to node 100, the master surface facet on element 10 is still the closest to the slave node. However, of the nodes defining facet 10, node 101 is closest to node 50 and therefore becomes the new tracked master surface node.

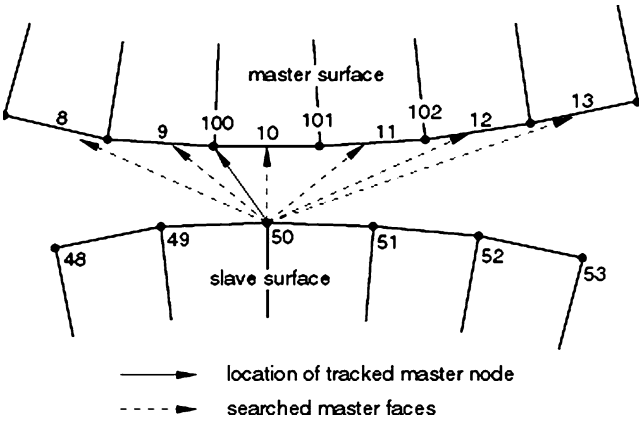

Fig. 1 A 2-D global search (ABAQUS Handbook, 2001)

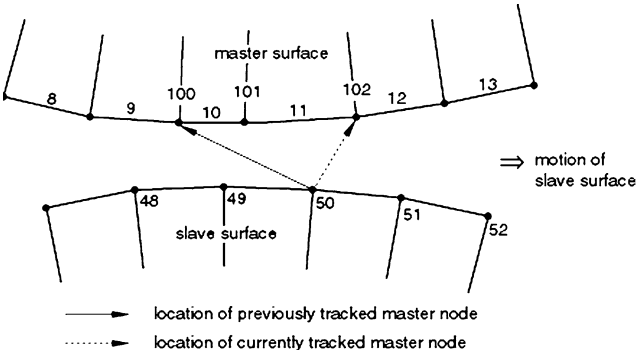

Fig. 2 A 2-D local search (ABAQUS Handbook, 2001)

If the tracked master surface node had remained node 100, then this would be the end of the procedure. However, because the master surface node has changed, the procedure continues. The second iteration finds the master surface facet on element 11 and the identity of the tracked master surface node is found to be node 102. The third and final iteration finds that the identity of the tracked master surface node does not change. A local search is less computationally expensive than a global search.

2.3. Adaptive meshing

Adaptive meshing is a tool that makes it possible to maintain a high quality mesh throughout an analysis, even when large deformations occur. This is achieved by allowing the mesh to move independently of the underlying material. The adaptive meshing technique in ABAQUS follows the work of Van Leer [25] and combines the features of a pure Lagrangian analysis and an Eulerian analysis. Therefore, it is often referred to as an ALE.

A smoother mesh is created by sweeping iteratively over the adaptive domain. During each mesh sweep, nodes in the domain are relocated based on the positions of neighbouring nodes and element centres. A volume smoothing technique is used to improve the quality of the mesh and one mesh sweep is performed after each increment. The mesh density near areas of evolving curvature is unchanged in this model.

In Fig. 3, the new position of node M is determined by taking the volume weighted average position of the element centres $C1$, $C2$, $C3$, and $C4$. The volume weighting will tend to push the node away from element centre $C1$ and toward $C3$. This can reduce the distortion of all four elements in Fig. 3.

2.4. Advecting solution variables to the new mesh

The ALE method of adaptive meshing introduces advective terms into the momentum balance and mass conservation equations. These account for the independent mesh and material motion. ABAQUS solves these modified equations by decoupling the material motion from the mesh motion. It has been proven that this technique has a high computational efficiency.

In an adaptive meshing increment, the element formulations, boundary conditions, external loads, contact conditions, etc. are all handled first in a manner consistent with a pure Lagrangian analysis. Once the Lagrangian motion has been updated and the mesh sweeps have been performed to find the new mesh, the solution variables are remapped by performing an advection sweep. Both momentum and field variables are advected during an advection sweep. A second order advection technique that is both monotonic and consistent is used to advect the field variables.

An element variable is remapped from the old mesh to the new mesh by first determining a linear distribution of the variable in each of the elements in the old mesh and

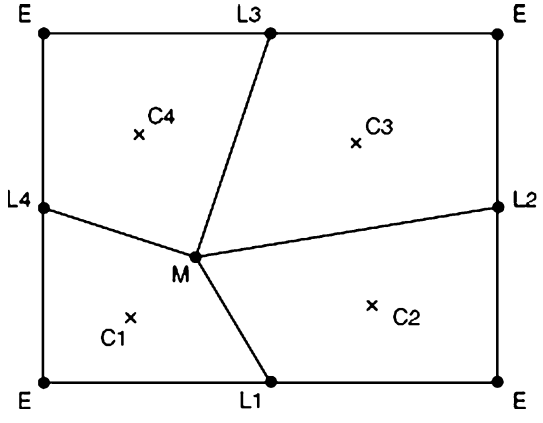

Fig. 3 Relocation of a node during a mesh sweep (ABAQUS Handbook, 2001)

advecting the distribution exactly. The process is described below for a one-dimensional element with one integration point. However, the process can easily be extended for two-dimensional elements.

The following technique is shown in Fig. 4:

- A quadratic function is constructed using the values of the variable at the integration points of a central element and its adjacent elements.
- A trial linear distribution of the variable is found by differentiating the quadratic function at the integration point of the central element.
- This trial linear distribution is limited by reducing its gradient until the minimum and maximum values are within the range of the element averages in the adjacent elements. This process is referred to as flux-limiting and is essential to ensure that the advection is monotonic.

Once the flux-limited linear distributions are determined for all elements in the old mesh, the distributions are integrated over each new element. The new values of the variable are found by dividing the value of each integral by each element volume.

Momentum advection is performed following the work of Benson [4]. Advecting momentum directly ensures that it is conserved properly during remapping and the method used in this simulation is known as the Half-Shift Index method. This method first shifts each of the nodal momentum variables to the element centre. The shifted momentum is then advected from the old mesh to the new mesh using the second order algorithm described previously. Finally, the momentum variables at the element centres of the new mesh are shifted back to the nodes.

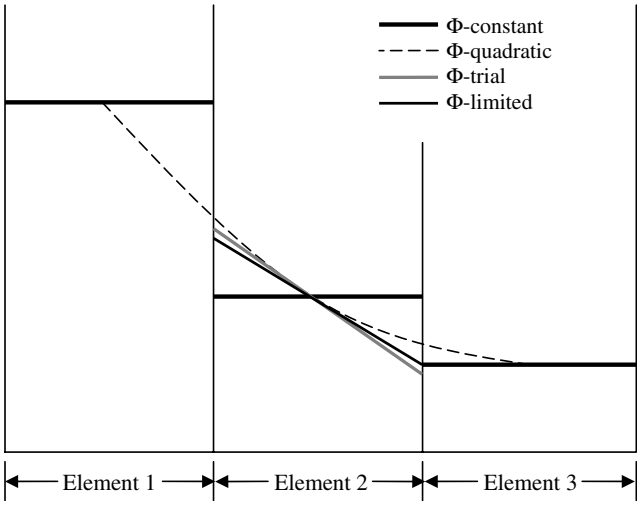

Fig. 4 Second order advection (ABAQUS Handbook, 2001)

3. Details of the analysis

3.1. Basic parameters

An axisymmetric model is used to simulate the deep penetration of a cone penetrometer in undrained clay.

The soil is approximated by a 1.5 m square domain whose mesh consists of 40,500 four-noded elements. A reduced integration scheme is used, i.e. one integration point is adopted for each element. This helps overcome the locking problem.

The area of the adaptive mesh is highlighted in Figure 5. This domain is 0.2m wide, 1.5 m deep and contains 27,000 elements. Boundary conditions place the fewest possible constraints on the mesh and are placed on both the bottom and left side of the mesh as shown in Fig. 5. In order to control the in situ stress conditions, loads are placed on both the top and the right side of the mesh. Different in situ stress states, soil strengths and roughnesses at the penetrometer–soil interface are modelled. The soil is modelled as an elastic perfectly plastic medium obeying the von Mises failure criterion and an associated flow rule. The analysis is performed using a total stress formulation and the effect of consolidation is not studied in detail here. The strength is varied by adjusting the rigidity index ($I_R = G/s_u$) so that the elastic modulus remains constant at 2.98 MPa and the Poisson's ratio is kept at 0.49 (to simulate incompressibility). Rigidity indices of 100, 300 and 500 are used in the simulations.

3.2. Hourglassing difficulties

Two unexpected difficulties may be encountered when performing the simulations. The first is the hourglassing of elements along the axis of symmetry ahead of the cone tip. This results in the elements becoming overly distorted and nodes slipping to the wrong side of the rigid analytical surface. This is shown in Fig 6. In this instance, hourglassing effects have distorted the elements ahead of the cone tip to the extent that one of nodes has crossed the axis of symmetry and remained in that position while the cone tip has passed it. Note that the node has not penetrated the cone surface.

For first order elements, ABAQUS uses an integration scheme that is based on the uniform strain formulation. This method was first proposed by Flanagan and Belytschko [10]. In this method, the strains are not calculated at the first-order Gauss points but are analytically calculated by averaging the strain over each element volume. For first-order elements, the uniform strain method yields the exact average strain over the element volume and lowers the computational cost of forming the element. However, the deficiency of reduced integration is that the

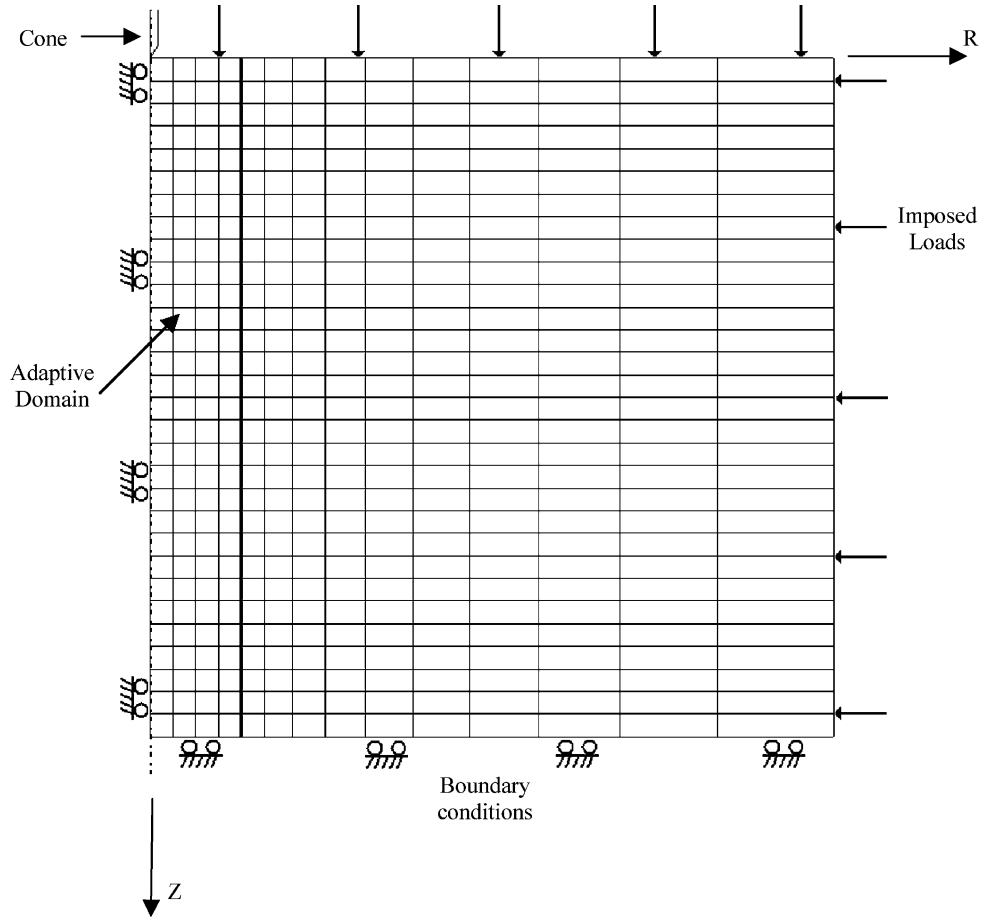

Fig. 5 A schematic of the finite element mesh

element stiffness matrix will be rank deficient and this will exhibit itself as hourglassing. This can make the elements unusable unless it is controlled. In ABAQUS, the artificial stiffness method developed by Flanagan and Belytschko [10] is used to control hourglassing by default. This method is generally successful in linear and mildly non-linear problems but breaks down in strongly non-linear problems and is not effective enough to be used in this model. Hence, a refinement of the hourglass control method is used. This approach is based on the enhanced assumed strain and physical hourglass control methods proposed in Engelmann and Whirley [9], Belytschko and Bindeman (1992) and Puso [20].

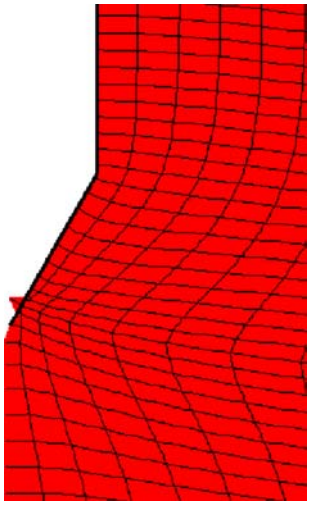

Fig. 6 The result of hourglassing

A finite element analysis of an axisymmetric footing problem has been performed to validate the model. A displacement controlled test forced the footing to penetrate 12% of its radius in a von Mises material which had an I_R of 100 and an undrained shear strength of 10 kPa. The finite element domain was square and 20 times the radius of the footing. The numerical results are presented in Fig. 7.

Following the method of characteristics, the exact bearing capacity of a circular footing resting on a Tresca material can be calculated as 5.69 su (See [22]). In the application of the theory by Shield [22], the hypothesis of Haar von Karman (1909) is assumed in the relevant plastic

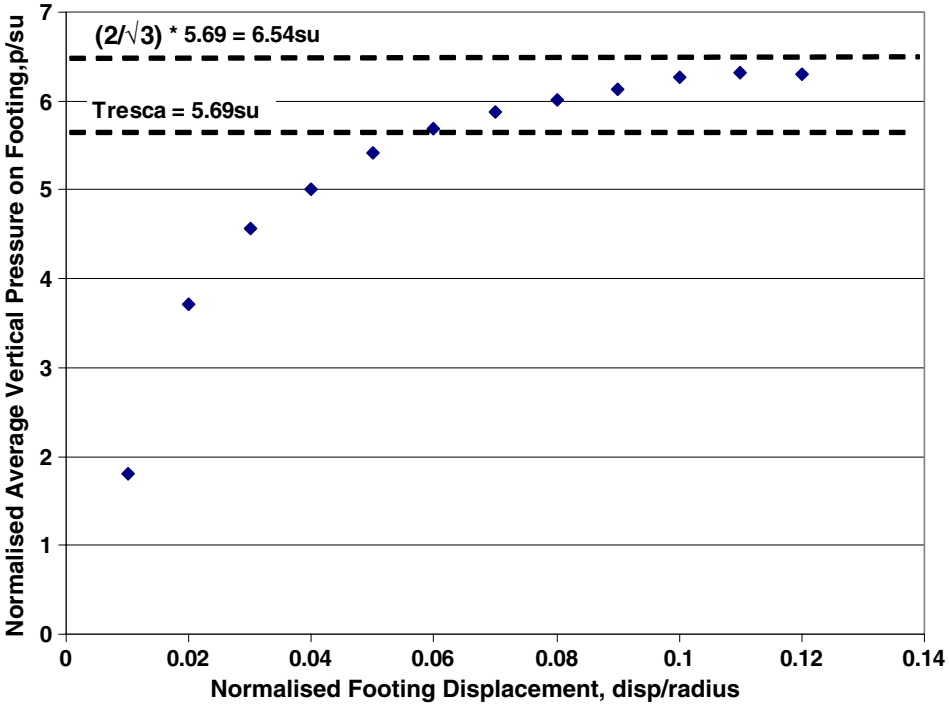

Fig. 7 Validation of finite elements using a smooth footing (IR = 100, s_u = 10 kPa)

state. This hypothesis states that the circumferential stress is taken to equal one of the other two principal stresses in the meridional plane. The validity of the Haar von Karman hypothesis in this situation arises directly from the use of the Tresca yield condition with an associated flow rule. When the von Mises yield condition is implemented, the analysis becomes more complex because the circumferential stress then depends on the strain pattern. The ratio of the maximum increase in strength given by the von Mises criterion over the Tresca criterion is approximately 15%. Hence, the increase in the resistance to penetration would be expected to be of this magnitude (i.e. $6.54s_u$). In Figure 7, it can be seen that the bearing capacity of the footing approaches this value.

3.3. Loading difficulties

The second difficulty arises when creating an in situ stress state in the mesh. This problem is the result of a software limitation that has been recognised by the producers. In the current release, ABAQUS/Explicit does not include initial stresses when calculating the initial accelerations. This is not a problem if the initial stress field is in static equilibrium with the external stresses, however, in other cases this may introduce noise into the solution.

The in situ stresses are created by externally loading the soil and the arrows in Fig. 5 represent the surfaces that are uniformly loaded to create the desired stress state. It is found that after the initial loading period, the values of the stresses within the mesh fluctuate even though the pressures at the boundaries are held constant. Clearly this causes the vertical stresses on the face of the cone to fluctuate during penetration. By reducing the rate at which the exterior loads are applied the fluctuation can be reduced, however; this can lead to impractically long run times. Instead, it has been found that the loads can be applied more quickly if they are smoothly increased. This can be understood using Fig. 8.

The sudden change in the rate of loading at the beginning and the end of the conventional loading step causes fluctuations in the in situ stress state. However, by using a smooth step this effect can be significantly reduced. The equation of the line representing the smooth loading in Figure 8 is given below;

$$a = a_i + (a_{i+1} - a_i)\xi^3(10 - 15\xi + 6\xi^2), \quad (1)$$

where

$$\xi = \frac{t - t_i}{t_{i+1} - t_i},$$

$t_i \leq t \leq t_{i+1}$ and 'a' represents the value of a field variable.

The simulation is performed using two steps. The first step lasts 25 s and during this step, the cone is held

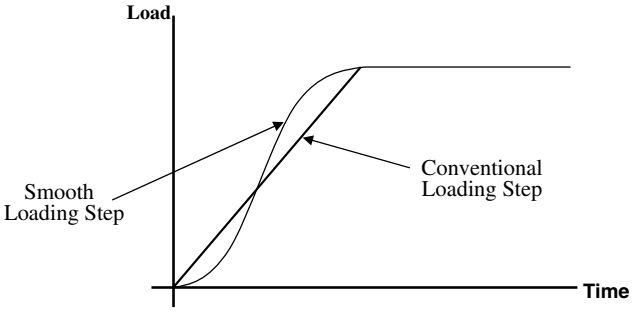

Fig. 8 Comparison of loading methods

stationary while loads are placed on the boundaries of the soil domain. This enables an in situ stress state to be set up before the penetration of the cone is carried out. The duration of the loading increment is 0.0005 s. This step can be omitted from analyses which have no initial in situ stress state.

The second step involves moving the cone to a penetration depth of 17 cone diameters (0.6069 m) whilst maintaining the loads placed on the boundaries. Adaptive meshing is used throughout this step to prevent over distortion of the elements adjacent to the cone. The duration of this step is 60.69 s and the loading increment is 0.0004 s. Five remeshing sweeps are performed after each increment. It has been found that increasing the size of the loading increment may lead to instability.

4. Results and discussions

4.1. Smooth conditions at the penetrometer-cone interface

In this section, the proposed numerical technique is applied to the cone penetration test in a weightless material. Sliding is allowed at the soil-penetrometer interface and no initial stress is imposed on the soil domain. In this case, the cone factor (Nc) is defined as the cone tip resistance (q) normalised by the undrained shear strength of the soil (s_u).

Figure 9 shows the evolution of the cone resistance as the cone penetrometer is pushed into three materials obeying the von Mises failure criterion. It can be concluded from Fig. 9, that it is not necessary to continue the analyses after a penetration depth of 17 diameters because a steady state condition has been reached.

The depth required to achieve a steady state condition increases with Ir. These results show that a steady state condition is achieved after a penetration depth of approximately 9 cone diameters in a von Mises material with an Ir of 100 and a steady state condition is achieved after a depth of approximately 15 cone diameters in a von Mises material with an Ir of 500. The final cone factors for the three different material stiffnesses are plotted on a logarithmic scale and are shown in Fig. 10.

The labels in Fig. 10 represent the cone factors at rigidity indices of 100, 300 and 500. The equation represents

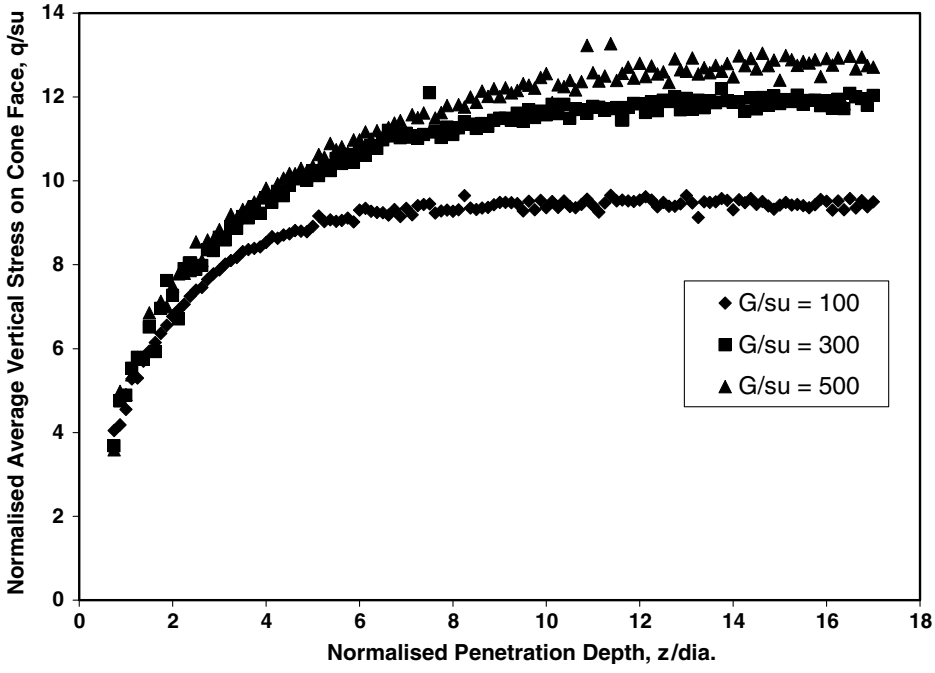

Fig. 9 Evolution of cone resistance in clays with different rigidity indices

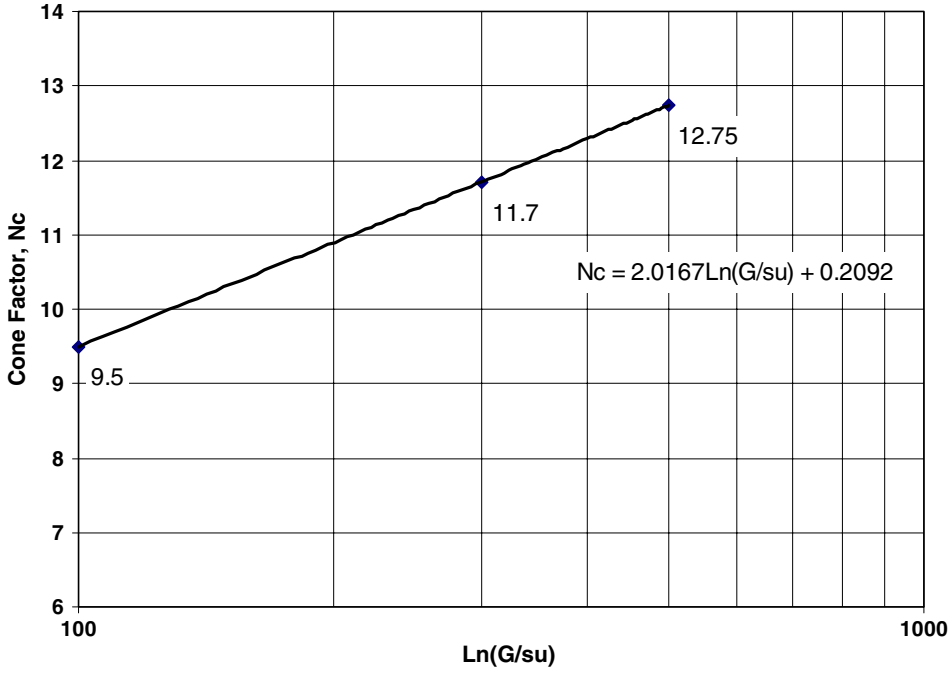

Fig. 10 Effect of the rigidity index on the cone factor

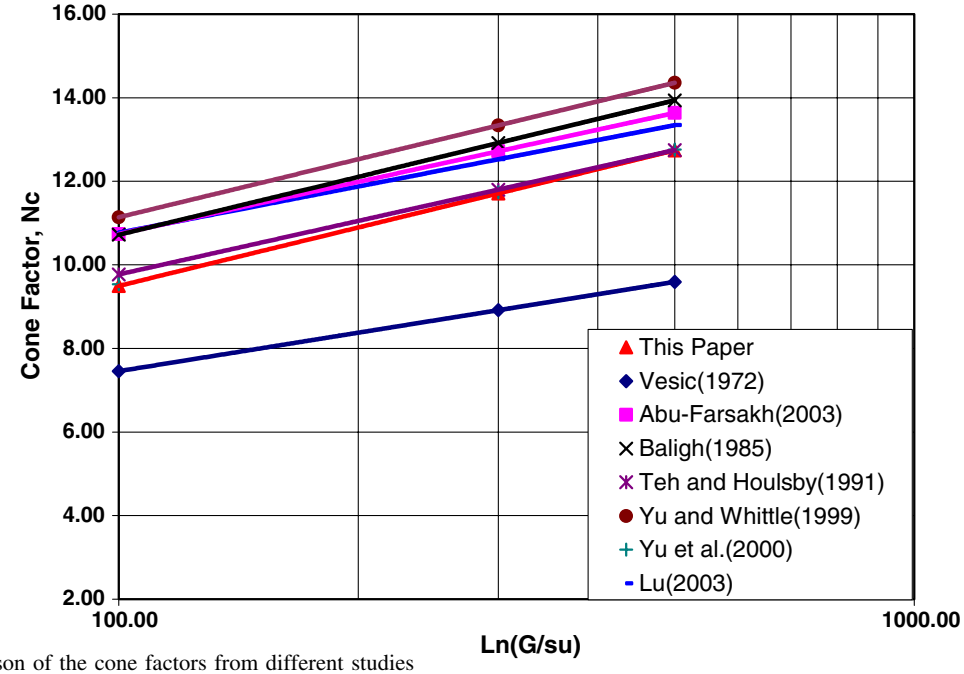

Fig. 11 Comparison of the cone factors from different studies

a fit to the numerical results. In order to validate these results, it is necessary to compare this equation with others, as shown in Fig. 11.

It can be seen that the result obtained using the proposed method agrees well with others. Of particular note is the extremely close agreement between the current work and Yu et al.'s (2000) novel method which can not be seen on the graph because the results virtually coincide with each other.

To further verify the numerical results, the distribution of the plastic strain is plotted at different stages of the analysis and it is shown in Fig. 12. The size of the plastic zone is then compared with solutions to cylindrical cavity expansion problems. It is found that the size of the plastic

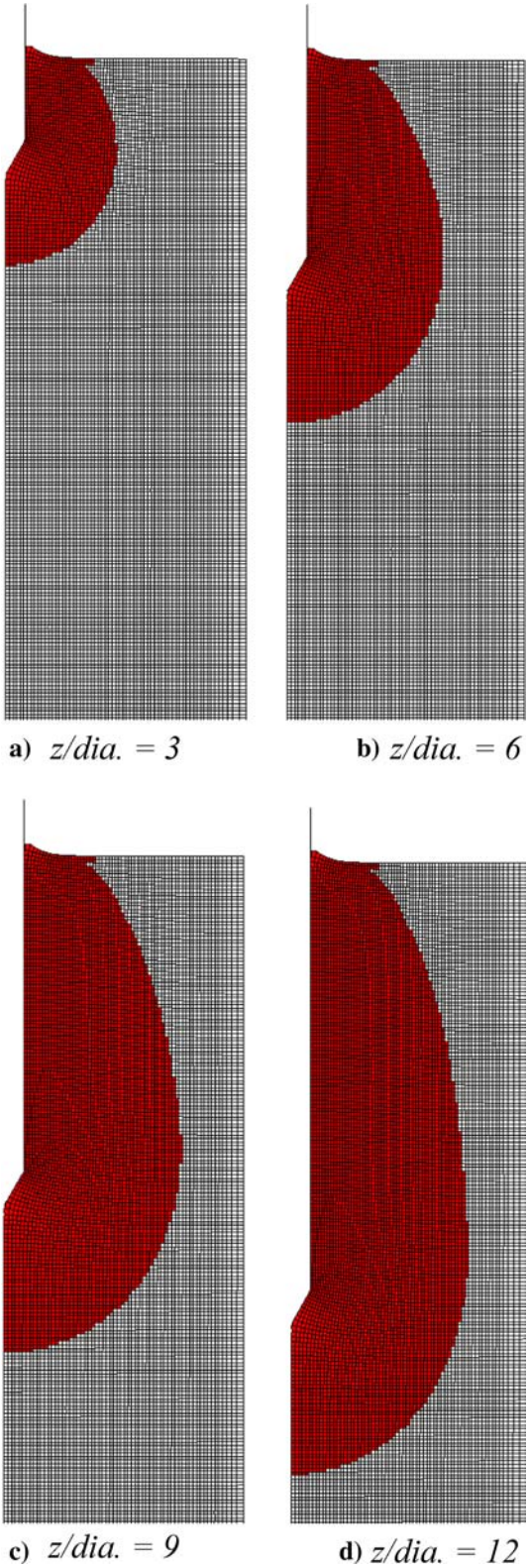

Fig. 12 Size of the plastic zone at different penetration depths

zone is 9.4 cone radii and this compares well with the cavity expansion solution which gives a value of 9.3 cone radii in a von Mises material with an IR of 100 [28].

4.2. Rough cone face and shaft

The investigation is extended to examine the effect of the roughness of the penetrometer on the cone factor. No special contact elements are needed because the explicit algorithm can handle complicated contact conditions (see sect 2.2). The friction conditions at both the cone face-soil interface and the shaft-soil interface are identical. It is assumed that the soil sticks to the penetrometer until the shear stress at the interface equals a predetermined fraction of the shear strength of the soil. At this point the material is allowed to slide freely. The maximum shear stress that can be reached in a von Mises material is given by:

$$\tau_{\max} = \frac{2s_u}{\sqrt{3}}, \tag{2}$$

where s_u is the undrained shear strength of the material under triaxial conditions.

Interface friction is proportional to the roughness of the cone penetrometer itself. Hence, to simulate different levels of roughness the maximum permissible shear stress at the interface is varied. The fraction of permissible shear stress at the interface can be described by the following equation:

$$\alpha = \frac{\tau_{\text{int}}}{\tau_{\max}}, \tag{3}$$

where τ_{int} is the permissible shear stress at the penetrometer-soil interface.

The final cone factors for four different values of α (=0, 1/3, 0.5, 2/3) are presented in Fig. 13 for three different rigidity indices (100, 300, 500).

It can be seen that the cone factor increases with friction at the interface. The four equations in Figure 13 represent the trend lines of the data and it can be seen that for the range of values considered, the inclusion of friction at the interface increases the gradient of the trends. Whilst the gradient is constant if friction is included, the intercept of each trend line varies with α and a curve fitting analysis has shown that the intercepts adhere to the following trend

$$\text{Intercept} = \alpha.(0.0026.(I_R) - 1.1919), \tag{4}$$

Hence the following relation is obtained for $1/3 \le \alpha_{cs} \le 2/3$.

$$N_c = 2.1907.\ln(I_R) + \alpha_{cs}.(0.0026.(I_R) - 1.1919). \tag{5}$$

where α_{cs} is the value of α at the penetrometer-soil interface. Many results in the literature use a linear term to describe the effect of the roughness of the penetrometer. However, the results in this paper show that this term is non-linear and dependent on IR.

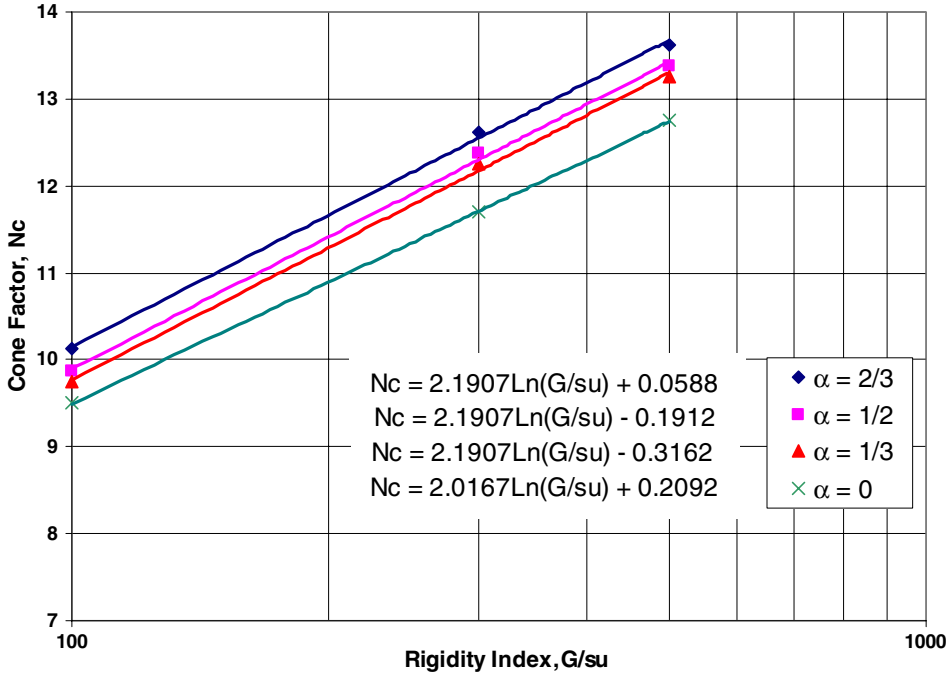

Fig. 13 Effect of a rough cone and shaft on the cone factor

4.3. Different friction conditions along the penetrometer

The study is extended further to examine the effect of a difference in the friction conditions at the cone face and the shaft. A penetrometer with both a smooth shaft and a rough cone face is simulated. Figure 14 shows the variation of the cone factor with both I_R and the roughness of the cone face.

It can be seen that Fig. 14 is identical to Fig. 13 and it appears that the inclusion of shaft friction has little effect on the results. This outcome was expected because it is unlikely that an increase in the shear stress in the

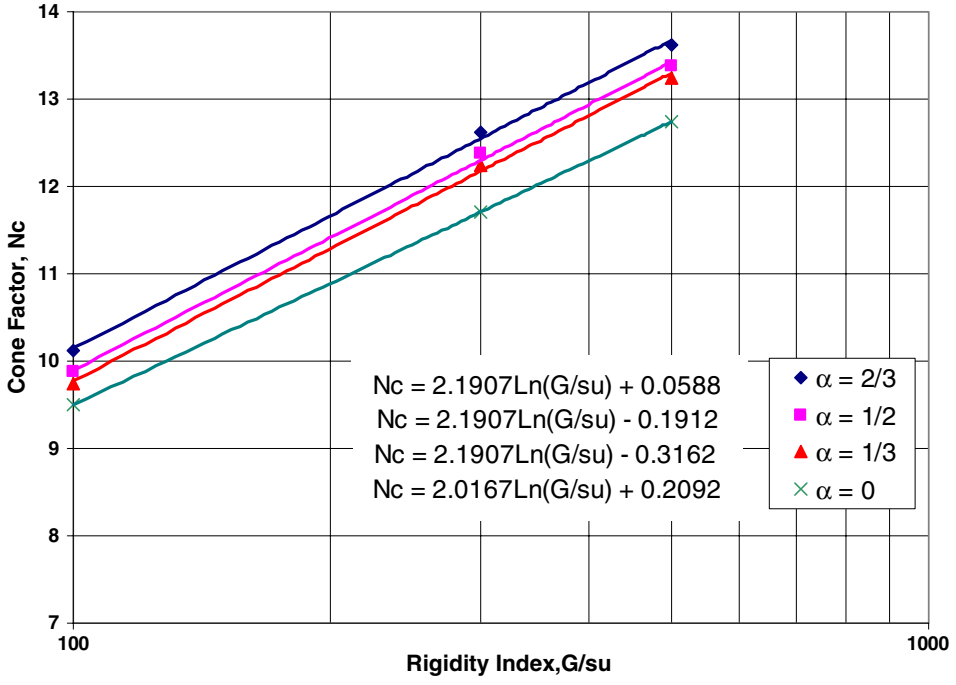

Fig. 14 Effect of a rough cone and a smooth shaft on the cone factor

material adjacent to the shaft would increase the mean stress ahead of the cone in a von Mises (non-dilatant) material. Other relevant results tend to place very little significance on the effect of the shaft friction. For example, Teh and Houlsby [23] use a value of $-0.2\alpha_s$ to account for the shaft friction (α_s is the roughness at the soil-shaft interface).

It should be noted that equation 5 can be used to describe the trends shown in Fig. 14 (with α_{cs} replaced with α_c, where α_c represents the roughness at the soil-cone face interface). These results emphasise the fact that the roughness of the cone face must be measured because the difference between the results neglecting the roughness at the cone face and those accounting for it, can be as high as 6.6%.

4.4. The effect of in situ stresses on the cone factor

To investigate the effect of the in situ stresses on the cone factor, the in situ stress state parameter is used (as defined by Teh and Houlsby [23]). This parameter, ranging between −1 and 1, is a measure of the in situ stress ratio.

$$\Delta = \frac{\sigma_{v0} - \sigma_{h0}}{2s_u}, \tag{6}$$

where σ_{v0} is the initial in situ vertical stress, σ_{h0} is the initial in situ horizontal stress and Δ is the anisotropic in situ stress parameter.

The final cone factors for different values of the in situ stress state parameter are presented in Fig. 15.

In simulations including an initial stress field, the following equations are used to calculate the cone factor:

$$N_{cv} = \frac{q - \sigma_{v0}}{s_u}, \tag{7a}$$

$$N_{ch} = \frac{q - \sigma_{h0}}{s_u} \tag{7b}$$

and

$$N_{cp} = \frac{q - \sigma_{p0}}{s_u}, \tag{7c}$$

where q is the average vertical pressure on the cone face and σ_{v0} is the vertical stress, σ_{h0} is the horizontal stress and σ_{p0} is the mean in situ pressure.

Five simulations are performed using a material with an I_R of 100. Similar tests performed in a material with an I_R of 300 will not change the trend of the results. Likewise, a test is performed at $\Delta = 0$ with a higher mean stress and no change in the cone factor results. The average vertical stress on the cone face is normalised by the vertical, horizontal or mean in situ stress to determine the relative importance of the in situ stresses to the cone resistance. It is found that the cone factor is more sensitive to changes in the initial stress ratio if the cone factor is normalised by the vertical stress. From Fig. 15, it can be seen that the gradient of the line that represents the

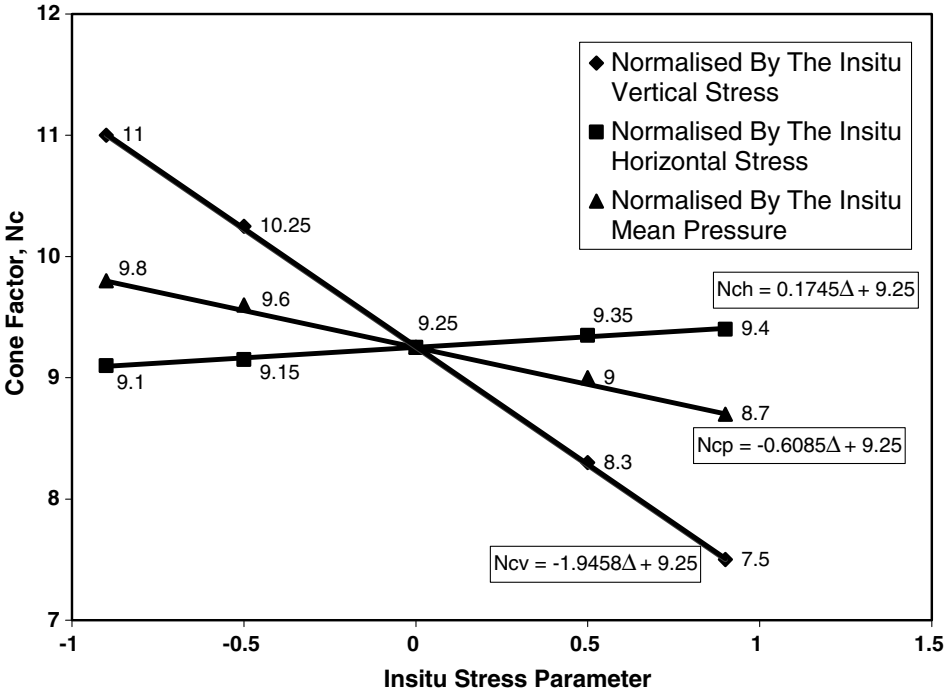

Fig. 15 Variation of the cone factor with the in situ stress state

Table 1 A Comparison of in situ Stress State Parameter Coefficients

Authors	*Coefficient*
Abu-Farsakh et al. [1]	2.1
Lu [18]	1.9
Teh and Houlsby [23]	2
Teh and Houlsby [23]	1.8
Yu et al. [32]	1.83
This paper	1.95

Table 2 Comparison of the cone factors

Author	IR		
	100	300	500
Abu-Farsakh et al. [1]	10.74	12.72	13.64
Baligh [2]	10.72	12.92	13.94
Lu [18]	10.77	12.53	13.34
Teh and Houlsby [23]	9.77	11.80	12.75
Vesic [26]	7.45	8.92	9.60
Yu and Whittle [31]	11.14	13.34	14.36
Yu et al. [32]	9.54	11.74	12.76
This paper	9.50	11.71	12.75

trend of these results has the value of −1.95. This is comparable to others in the literature and these are summarised in Table 1.

The gradient of −1.95 is found for the values $-0.9 \le \Delta \le 0.9$. This investigation shows that difficulties arise when performing the simulations under initial stress conditions at, or approaching, $\Delta = \pm 1$. A typical result is presented in Fig. 16.

In Figure 16 it can be seen that after the initial penetration the cone factor reduces with depth. This effect can be investigated by changing the loading increment, the boundary conditions and the number of elements. It seems that this effect is caused by the material unloading during the penetration. This is possible because the material is in a plastic state at the beginning of the simulation and the penetration itself causes parts of the soil to unload and become elastic, i.e. at the start of the simulation, every point in the material is on the yield surface and the stress paths can only move along or inside the yield surface.

Provided that the cone factor is found by normalising the vertical force on the cone face by the in situ vertical stress, the following equation can be used under the conditions of $1/3 \le \alpha_{cs} \le 2/3$ and $-0.9 \le \Delta \le 0.9$ to relate the cone factor to the soil properties.

$$N_c = 2.19.\ln(I_R) + \alpha_{cs}.(0.0026.(I_R) - 1.1919) - 1.95\Delta. \quad (8)$$

If the penetrometer is completely smooth then the following relation can be used

$$N_c = 2.02.\ln(I_R) - 1.95\Delta. \quad (9)$$

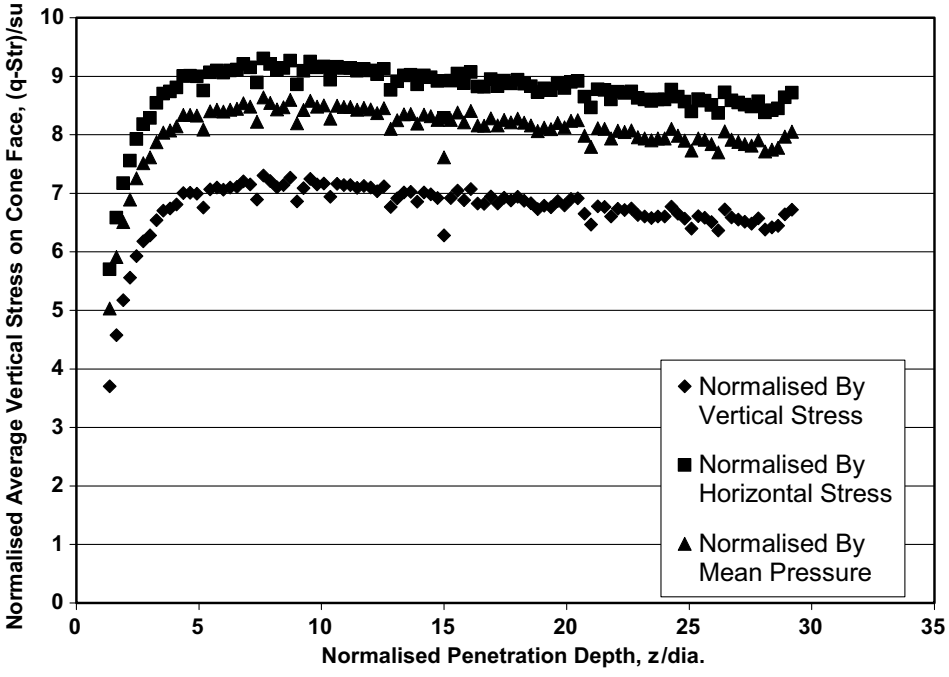

Fig. 16 Strain softening in a von Mises material (IR = 100, s_u = 10 kPa, Δ = 1.0)

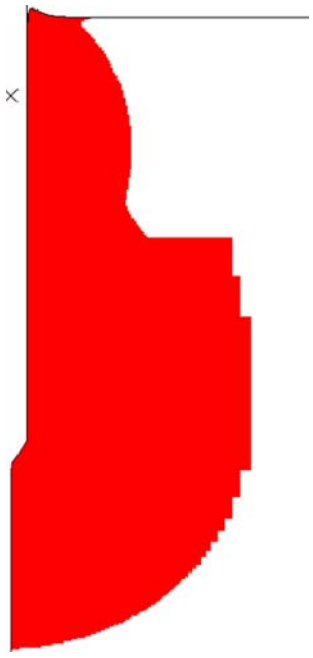

Fig. 17 Plastic area in a two-layered clay

4.5. Further Work

In order to demonstrate this numerical technique further, Fig. 17 shows the plastic zone around a cone that has been pushed through a multi-layered clay. This clay is modelled using the von Mises failure criterion. The upper material has an I_R of 100 and the bottom material has an I_R of 300. Both materials have a shear modulus of 1 MPa. The radii of the plastic zone is 7.75 diameters and 15.375 diameters in the top and bottom materials respectively. The interface between these materials is at a depth of 0.3 m (8.4 cone diameters) and this is represented by the vertical line in Fig. 18. Figure 18 shows the vertical pressure on the cone face during the penetration process. A predictive response can be seen because the vertical resistance to the penetration reduces before the cone penetrates the softer soil. This is a demonstrative example of our ongoing work which further utilises the proposed method.

5. Conclusion

An explicit finite element model based on the commercial code ABAQUS has been developed to simulate the cone penetration test in undrained clay using the von Mises yield criterion. An explicit integration scheme with an adaptive meshing algorithm enables the simulation to run continuously. The dependency of the cone factor on I_R, penetrometer roughness and the in situ stress state has been evaluated. The advantages of the proposed numerical method are as follows:

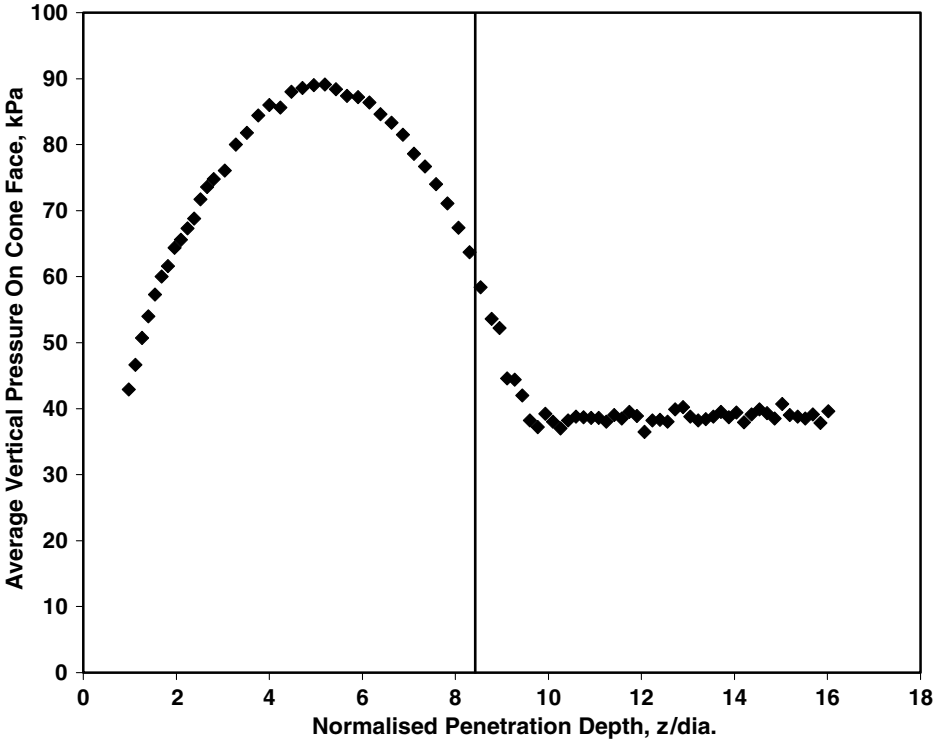

Fig. 18 Vertical resistance vs. cone penetration depth. (IR = 100(top layer): IR = 300(bottom layer), G = 1 MPa)

- An explicit integration scheme efficiently performs a large number of increments and simplifies the treatment of contact.
- The cone geometry can be modeled explicitly and no special contact elements are required at the penetrometer-soil interface.
- The roughness at the shaft-soil and cone face-soil interface can be varied independently.
- The approach can easily be extended for the analysis of the cone penetration test in frictional-dilatant materials.
- Accurate results can be obtained using first order elements.

The proposed numerical method provides an effective tool for the analysis of the cone penetration test. Furthermore, this method can be extended to the analysis of the cone penetration test in frictional-dilatant soils. Preliminary tests have shown that this model is capable of achieving good results in these materials.

Acknowledgements The authors would like to thank Dr. Huaxiang Li of the Nottingham Centre for Geomechanics for his valuable assistance during the course of this work.

References

1. Abu-Farsakh M, Tumay M, Voyiadjis G (2003) Numerical parametric study of.piezocone penetration test in clays. Int J Geomech 3(2):170–181
2. Baligh MM (1985) Strain path method. J Geotech Eng, ASCE 111(3):1108–1136
3. Belytschko T, Bindeman LP (1993) Assumed strain stabilization of the eight node hexahedral element. Comp Methods in Appl Mech Eng 105:225–260
4. Benson DJ (1992) Momentum advection on a staggered mesh. J of Comput Phys 100:143–162
5. Budhu M, Wu CS (1992) Numerical analysis of sampling disturbances in clay soils. Int J Numer Anal Methods in Geomech 16:467–492
6. Cheng JH (1988) Automatic adaptive remeshing for finite element simulation of forming processes. Int J Numer Methods in Eng 26:1–18
7. Cividini A, Gioda G (1988) A simplified analysis of pile penetration. Proc 6th Int Conf on Numer Methods in Geomechanics, pp 1043–1049
8. De Borst R, Vermeer PA (1984) Finite element analysis of static penetration tests. Geotechnique 34(2):199–210
9. Engelmann BE, Whirley RG (1990) A new explicit shell element formulation for impact analysis. In: Kulak RF, Schwer LE (eds) Computational aspects of contact, impact and penetration. Elmepress International
10. Flanagan DP, Belytschko T (1981) A uniform strain hexahedron and quadrilateral with orthogonal hourglass control. Int J Numeric Methods in Eng17:679–706
11. Haar von Karman Th (1909) Nachr Ges WissGöttingen Math-Phys Kl 204
12. Houlsby GT, Wheeler AA, Norbury J (1985) Analysis of undrained cone penetration as a steady flow problem. Proceedings of the fifth International Conference on Numerical Methods in Geomechanics 4:1767–1773
13. Hu Y, Randolph MF (1998) A practical numerical approach for large deformation problems in soil. Int J Numeric Anal Meth Geomech 22(5):327–350
14. Huetink J (1982) Analysis of metal forming process based on a combined Eulerean-Lagrangean finite element formulation. Proceedings of the International Conference on Numerical Methods for Industrial Forming Processes, Pineridge, Swansea, U.K, pp 501–509
15. Huetink J (1986) On the simulation of thermomechanical forming processes. PhD Thesis University of Enschede, The Netherlands
16. Kiousis PD, Voyiadis GZ, Tumay MT (1988) A large strain theory and its application in the analysis of the cone penetration mechanism. Int J Numeric Anal Methods Geomech12:45–60
17. Lee NS, Bathe KJ (1994) Error indicators and adaptive remeshing in large deformation finite element analysis. Finite element analysis in design 16:99–139
18. Lu Q (2003) A numerical study of penetration resistance in clay. PhD Thesis, The University of Western Australia
19. Lunne T, Robertson PK, Powell JJM (1997) Cone penetration testing. E&FN Spon, London
20. Puso MA (2000) A highly efficient enhanced assumed strain physically stabilized hexahedral element. Int J Numeric Methods in Eng49:1029–1064
21. Sheng D, Axelsson K, Magnusson O (1997) Stress and strain fields around a penetrating cone. Proceedings of the sixth International Symposium on Numerical Models in Geomechanics. NUMOG-VI (Montreal, Canada), pp 456–465
22. Shield RT (1955b) On the plastic flow of metals under conditions of axial symmetry. Proceedings of the Royal Society for Maths and Physics 233(A):267–287
23. Teh CI, Houlsby GT (1991) An analytical study of the cone penetration test in clay. Geotechnique 41(1):17–34
24. Van den Berg P (1994) Analysis of soil penetration, PhD Thesis, Delft University
25. Van Leer B (1977) Towards the ultimate conservative difference scheme III. Upstream-centred finite-difference schemes for ideal compressible flow. J of Comput Phys 23:263–275
26. Vesic AS (1972) Expansion of cavities in an infinite soil mass. J Soil Mech Found Div ASCE 98:265–290
27. Wroth CP (1984) The interpretation of in situ soil test. 24th Rankine lecture, Geotechnique 1984 34(4):449–489
28. Yu HS (2000) Cavity expansion methods in Geomechanics. Kluwer, Dordrecht
29. Yu HS (2004) In situ soil testing: From mechanics to interpretation. First James K. Mitchell Lecture, Proc ISC-2 on Geotechnical and Geophysical Site Characterization, Viana da Fonseca & Mayne, 2004 Millpress, Rotterdam, 1:3–38
30. Yu HS, Mitchell JK (1998) Analysis of cone resistance: review of methods. J Geotech and Geoenvironment Eng, ASCE 124(2):140–149
31. Yu HS, Whttle AJ (1999) Combining strain path analysis and cavity expansion theory to estimate cone resistance in clay. Unpublished Notes
32. Yu HS, Herrmann LR, Boulanger RW (2000) Analysis of steady cone penetration in clay. J Geotech Geoenvironment Eng, ASCE 126(7):594–605